

Tuning Deazaflavins Towards Highly Potent Reducing Photocatalysts Guided by Mechanistic Understanding – Enhancement of the Key Step by the Internal Heavy Atom Effect

Tetiana Pavlovska,^[a] David Král Lesný,^[a] Eva Svobodová,^[a] Irena Hoskocová,^[b] Nataliya Archipowa,^[c] Roger Jan Kutta,^{*,[d]} and Radek Cibulka^{*,[a]}

Abstract: Deazaflavins are well suited for reductive chemistry acting via a consecutive photo-induced electron transfer, in which their triplet state and semiquinone – the latter is formed from the former after electron transfer from a sacrificial electron donor – are key intermediates. Guided by mechanistic investigations aiming to increase intersystem crossing by the internal heavy atom effect and optimising the concentration conditions to avoid unproductive excited singlet reactions, we synthesised 5-aryldeazaflavins with Br or Cl substituents on different structural positions via a three-

component reaction. Bromination of the deazaisoalloxazine core leads to almost 100% triplet yield but causes photoinstability and enhances unproductive side reactions. Bromine on the 5-phenyl group in ortho position does not affect the photostability, increases the triplet yield, and allows its efficient usage in the photocatalytic dehalogenation of bromo- and chloroarenes with electron-donating methoxy and alkyl groups even under aerobic conditions. Reductive powers comparable to lithium are achieved.

Introduction

Recent developments in photoredox catalysis have substantially affected synthetic chemistry by providing photocatalytic counterparts to traditional methods that even significantly overcome their limitations.^[1–2] In photoredox catalysis, an excited photocatalyst – usually an organic dye or transition-metal complex –

initiates a single electron transfer (SET) from/to the substrate, forming a radical species, which undergoes a desired transformation.^[3] Simultaneously, the additional energy of light absorbed by a photocatalyst allows redox chemical processes, which are inaccessible in the dark. In reductive photocatalysis, the generation of aryl radicals represents one of the most important achievements. Such radical species can be trapped with a suitable reagent to form C–C and C-heteroatom bonds.^[4] Originally, activated compounds like aryl diazonium or iodonium salts, but not the commercially available halides, were used as aryl radical sources in photocatalysis.^[4a,5] Although there is a particular success in photoreduction of aryl iodides, some aryl bromides, and aryl chlorides, that are activated by an electron-withdrawing group,^[6] the reduction of non-activated aryl halides remains challenging.

The redox potentials, E^* , of the strongest reducing photocatalysts in an excited state range between -2 V and -2.2 V vs. SCE (saturated calomel electrode) even after structure optimisations,^[6a,7–8] which are insufficient for challenging substrates like 4-bromoanisole and 4-chloroanisole with $E_{\text{red}} = -2.75$ V and -2.88 V (values from ref.^[4c]), respectively (see Figure 1a). Recently, reduction of non-activated and deactivated aryl bromides or chlorides was achieved by either consecutive photo-induced electron transfer (conPET) or photo-electrochemistry (Figure 1b).^[9] In these transformations the reducing power of the excited state of either radical anions or neutral radicals is used. The radical species are formed either by PET from a sacrificial electron donor (S_{sa}) to the excited photocatalyst,^[4c,10–13] or without light by reduction of the photocatalyst on an electrode.^[14–15] However, so far, naphthalene imide **4**,^[14] dicyanoanthracene **5**,^[15] acridinium salt

[a] Dr. T. Pavlovska, D. Král Lesný, Dr. E. Svobodová, Prof. Dr. R. Cibulka
Department of Organic Chemistry
University of Chemistry and Technology, Prague
Technická 5, 166 28, Prague 6
(Czech Republic)
E-mail: cibulka@vscht.cz

[b] Dr. I. Hoskocová
Department of Inorganic Chemistry
University of Chemistry and Technology, Prague
Technická 5, 166 28, Prague 6
(Czech Republic)

[c] Dr. N. Archipowa
Institute for Biophysics and Physical Biochemistry
University of Regensburg
D-93053 Regensburg (Germany)

[d] Dr. R. J. Kutta
Institute of Physical and Theoretical Chemistry
University of Regensburg
D-93053 Regensburg (Germany)
E-mail: roger-jan.kutta@chemie.uni-regensburg.de

Supporting information for this article is available on the WWW under <https://doi.org/10.1002/chem.202200768>

© 2022 The Authors. Chemistry - A European Journal published by Wiley-VCH GmbH. This is an open access article under the terms of the Creative Commons Attribution Non-Commercial NoDerivs License, which permits use and distribution in any medium, provided the original work is properly cited, the use is non-commercial and no modifications or adaptations are made.

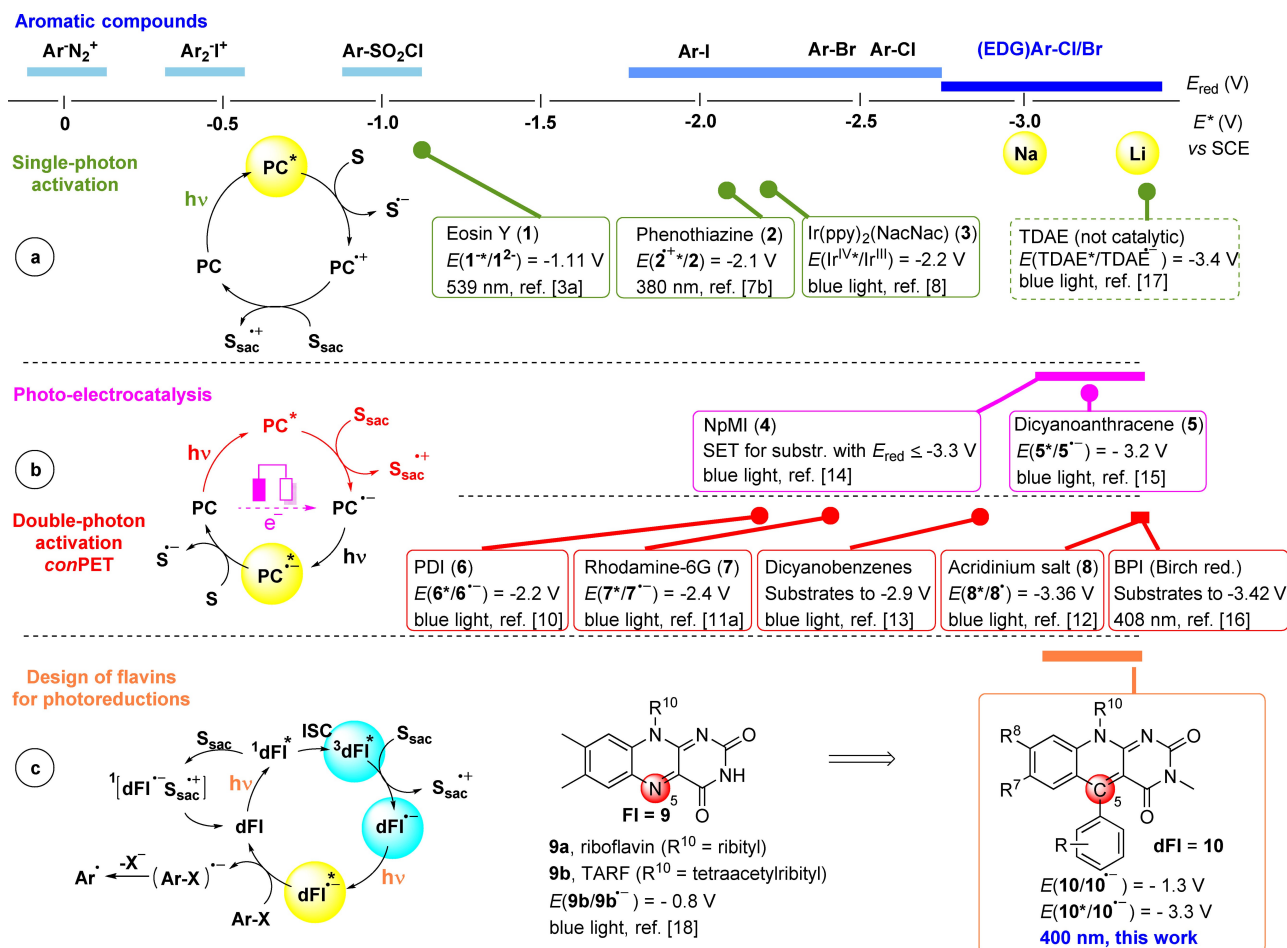


Figure 1. Overview of the strongest species in the excited state and schemes of their generation. Selected examples of reductants are shown for less powerful systems ($E^* > -3$ V). Values $E(M^+/M)$ for sodium and lithium are taken from ref. [24]. Abbreviations: SET – single electron transfer; EDG – Electron Donating Group; PC – photocatalyst; S – substrate; S_{sac} – sacrificial electron donor; Ar – Aryl; ppy – 4-(1-pyrrolidinyl)pyridine; NacNac – β -diketiminato ligands; TDAE – tetrakis(dimethylamino)ethylene; NpMI – naphthalene-based analogue; PDI – perylene diimide; BPI – benzo[ghi]perylene monoimide.

8,^[12] and benzo[ghi]perylene monoimide (BPI) derivatives^[16] are the only photocatalysts that allow the reduction of substrates with E_{red} around -3 V via an excited state radical. To note, excited tetrakis(dimethylamino)ethylene (TDAE) is also capable to reduce substrates with $E_{red} < -3$ V, but the reported dehalogenation is not catalytic.^[17] Hence, the development of novel photocatalysts with high reductive power for mild and efficient aryl radical generation of the wide range of aryl halides is of high interest.

Within the last decades, flavins (FI), derivatives of flavin mononucleotide (FMN), flavin adenine dinucleotide (FAD), or riboflavin, have been recognised as beneficial photocatalysts for oxidations.^[18–19] However, only rare examples of flavin-based photocatalytic reductive processes are reported.^[20–21] The structurally similar 5-deazaflavins (dFI), where the N-5 of the flavin isoalloxazine moiety is replaced by a methine group (Figure 1c, position 5 is highlighted), are better suited for reductive chemistry due to their more negative reduction potential (ca. -1.3 V vs. SCE). However, dFIs are usually involved in two-electron reductions, both, in natural and artificial systems, owing to the low stability of the semiquinone (dFI $^{\cdot-}$)

formed by a one-electron reduction.^[22] Direct evidence for the involvement of deazaflavin semiquinone radicals in a reductive process was missing until recently. We proved the formation of the deazaflavin semiquinone by PET from the electron donor *N,N*-diisopropylethylamine (DIPEA) to the triplet state of the dFI, while the reaction with the excited singlet state results in a spin-correlated radical pair which is spin-allowed for recombination and, thus, represents a complete loss channel of the excitation energy. The radical can be excited by a second photon to form an extremely strong reducing species allowing the reduction of 4-bromoanisole and even 4-chloroanisole.^[23]

Here, we present a comprehensive investigation of the 5-aryldeazaflavin reactivity in model dehalogenation reactions with the special focus on non-activated and deactivated substrates with very negative reduction potentials. Since the first crucial intermediate in the productive reaction mechanism is the triplet state of dFI, we aimed to enhance the intersystem crossing (ISC) by increasing the spin-orbit coupling (SOC) via – at least in principle – introduction of a heavy atom into the dFI manifold. Hence, we designed and prepared a series of 5-aryldeazaflavin derivatives 10 via three-component reactions in

which a bromine is located at different structural positions. In order to elucidate the heavy atom effect on the photophysics and photocatalytic reactivity, the results were compared with those of the corresponding chlorinated **dFI** derivatives. Furthermore, as the diffusion-controlled reaction with the sacrificial electron donor can occur either with the excited singlet or triplet state of **dFI** forming spin-correlated radical pairs, we optimised the concentration conditions for maximal avoidance of the unproductive reaction via the excited singlet state. This allowed us to elucidate a structure vs. conditions vs. catalytic activity relationship and to develop extremely strong reducing agents comparable to sodium and lithium.

Results and Discussion

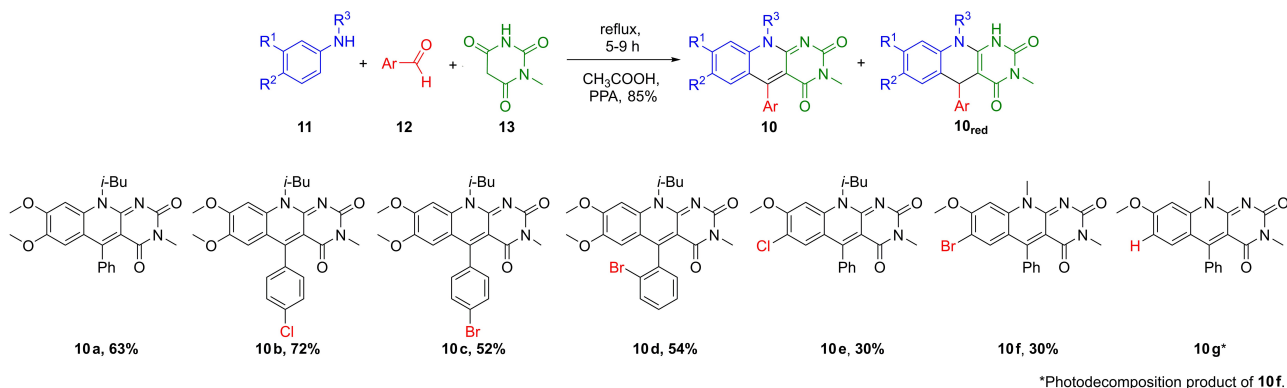
Design and synthesis of the 5-aryldeazaflavins. In our previous study^[23] we have shown that the 5-aryl and 7,8-methoxy groups have a positive effect on the photocatalytic activity/reduction potential of deazaflavins. Thus, this was considered in the design of the new photocatalysts with either a chlorine or a bromine located either on the deazaaisoalloxazine core or on the phenyl ring. Several methods can be applied for the synthesis of the 5-deazaflavins, which include the condensations of anthranil aldehydes with barbituric acid or 6-chloro-3-methylpyrimidine-2,4(1*H*,3*H*)-dione with aryl aldehydes.^[25] However, these approaches are not suitable for the involvement of the aryl substituent in position 5 of the deazaaisoalloxazine core. Our previously developed microwave-assisted three-component reaction between benzaldehyde, *N*-butyl-3,4-dimethoxyaniline, and *N*-methylbarbituric acid without additional solvent, yielded both, the oxidised and fully reduced, forms in the combined yield of 20%.^[23] However, we noticed that the presence and chemical nature of the solvent is highly important for this reaction. Inspired by the pioneering work by Yoneda,^[25c] we have significantly improved our approach by performing a three-component condensation between *N*-alkyl anilines **11** (Note, that in the present study the isobutyl group at N-10 is used instead of the previously described *n*-butyl derivative. This modification does not influence the photocatalyst activity.), aromatic aldehydes **12**, and *N*-methylbarbituric acid (**13**) in

AcOH/PPA (polyphosphoric acid) resulting in 5-aryldeazaflavins **10_{ox}** and **10_{red}** in overall moderate to high yields (Scheme 1 and Figure S1; see Supporting Information for details). To note, the amount of the reduced forms of compounds **10a** (-H), **10c** (*p*-Br), and **10f** (*iso*-Br) was lower than 10%, so that only the oxidised 5-deazaflavins were isolated. However, in the absence of PPA and under inert atmosphere, the reduced forms **10a_{red}**, **10b_{red}** (*p*-Cl), **10c_{red}**, and **10f_{red}** were formed as major products and were obtained in pure form by recrystallisation from propan-2-ol.

General photocatalytic performance of **dFI **10** in the dehalogenation.** Based on our previous study, the acid-base equilibrium of the deazaflavin semiquinone impacts on the overall performance of the dehalogenation, since the deprotonated form seems to be beneficial potentially due to: 1) an enhanced triplet yield; 2) a longer triplet lifetime; 3) an enhanced **dFI**^o yield; or 4) longer lifetime of **dFI**^o.^[23] Detailed studies on the impact of the basicity on the reaction mechanism are currently ongoing in our lab. However, here we focus on enhancing the ISC by an internal heavy atom effect (IHA) and, thus, we performed all photocatalytic experiments under the most efficient conditions as previously described, i.e. in the presence of caesium carbonate (Cs₂CO₃) as a base and at 6 mM (8 mol%) **dFI** **10**.^[23] Similar to our previous results, a lower concentration of the novel **dFIs** results in a lower product yield (see Scheme S4 in the Supporting Information).

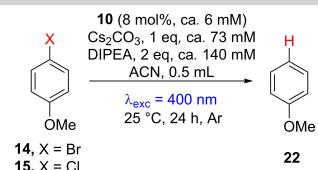
Initially, the performance of the synthesised 5-aryldeazaflavins **10** in the dehalogenation of 4-bromoanisole (**14**) and 4-chloroanisole (**15**) (Table 1) was explored. Most of the 5-aryldeazaflavin derivatives were capable of debrominations and dechlorinations with high to quantitative yields. Interestingly, derivatives **10e** (*iso*-Cl) and **10f** (*iso*-Br) with halogen atoms on the deazaaisoalloxazine core performed less efficient compared to the other **dFI** **10** particularly in terms of the dechlorination of **15**. In the absence of the photocatalyst no formation of the respective anisole **22** was observed.

Importantly, the **dFIs** **10a–d** even allowed the conversion of bromo- and chloroarenes **16–21** whose reduction is highly deactivated owing to electron-donating methoxy and alkyl groups (Table 2). The best performance was observed for the debromination of 1-bromo-2,4-dimethoxybenzene (**16**) using



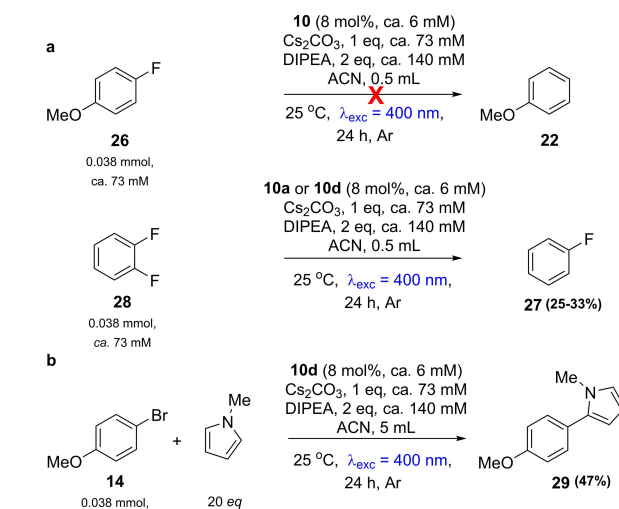
Scheme 1. Synthesis of 5-aryldeazaflavins **10**. Yields of isolated products are given.

Table 1. Dehalogenation of 4-bromo-(**14**) and 4-chloroanisoles (**15**) catalysed by dFI **10**.^[a]

		
Catalyst	Yields [%]	
	14	15
10a (-H)	98	82
10b (p-Cl)	89	90
10c (p-Br)	93	70
10d (o-Br)	98	99
10e (iso-Cl)	95	31
10f (iso-Br)	37	6
10g (iso-H)	64	n.d.
–	< 1	0

[a] **Reaction conditions:** **14** or **15** (0.038 mmol, ca. 73 mM), **10** (0.003 mmol, ca. 6 mM), DIPEA (0.072 mmol; ca. 140 mM), ACN (0.5 mL), Cs₂CO₃ (0.038 mmol, ca. 73 mM), T = 25 °C, argon atmosphere, λ_{exc} = 400 nm, t_{rea} = 24 h. n.d. = not determined.

the photocatalysts **10a–d** and for 1-bromo-2,4,6-trimethoxybenzene (**18**) using the photocatalysts **10a** and **d**. In these cases, the conversion was almost quantitative. Furthermore, the novel dFI **10** catalysed the dehalogenation of aryl chlorides such as 1-chloro-2,4,6-trimethoxybenzene (**19**) and 3,5-di-*tert*-butyl-1-chloroanisole (**21**) ($E_{\text{red}} = -3.4 \text{ V}^{[14]}$) as well as its bromo analogue **20** albeit in moderate yields. However, defluorination of 1-fluoro-4-methoxybenzene (**26**) could not be achieved by dFI **10**. To the best of our knowledge, no photocatalytic system capable to defluorinate **26** is reported so far. Anyhow, we observed the defluorination of 1,2-difluorobenzene (**28**) in the presence of either **10a** (-H) or **10d** (o-Br) (Scheme 2a). Furthermore, the dFI **10** can also be used in coupling reactions

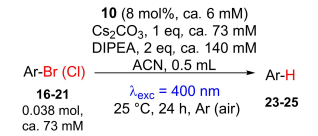


Scheme 2. (a) (In)ability of dFI **10** to defluorinate 1-fluoro-4-methoxybenzene (**26**, upper) and 1,2-difluorobenzene (**28**, lower). (b) Exemplary coupling reaction between 4-bromoanisole (**14**) and *N*-methylpyrrole catalysed by dFI **10d**.

as is exemplarily shown on the reaction of **14** with *N*-methylpyrrole (Scheme 2b, see Supporting Information for details).

Moreover, in order to avoid undesired reactions between the radical intermediates and molecular oxygen, reductive chemistry using photoredox catalysis or photo-electrochemistry is usually performed under strictly inert conditions. Interestingly, the reductive photodehalogenation catalysed by **10** can also be performed under aerobic conditions resulting in only slightly reduced yields in comparison to inert conditions after 24 h of illumination (Table 2). However, it should be noted that after 1 h of illumination, the photodehalogenation reaction under aerobic conditions is only half as efficient as compared to

Table 2. Dehalogenation reactions with selected electron-rich aromatic halides.^[a]

						
Substrate	Product	Catalyst	Yields ^[b] [%]			
	23			24	25	21
16		10a (-H)	99	92 (60 ^[c])	74 (68 ^[c])	31
17		10b (p-Cl)	99	53	50	52
18		10c (p-Br)	97	55	35	47
19		10d (o-Br)	98	96 (80 ^[c])	22	65
20				36	67 (62 ^[c])	24
21						

[a] **Reaction conditions:** substrate (0.038 mmol, ca. 73 mM), **10** (0.003 mmol, ca. 6 mM), DIPEA (0.072 mmol, ca. 140 mM), ACN (0.5 mL), Cs₂CO₃ (0.038 mmol, ca. 73 mM), T = 25 °C, argon (air) atmosphere, λ_{exc} = 400 nm, t_{rea} = 24 h. [b] Yields determined via HPLC for **23** and via ¹H NMR for **24** and **25**. [c] Data in parenthesis are from experiments under aerobic conditions.

the inert conditions (see Scheme S2). Since under the used photocatalytic conditions, the DIPEA concentration is significantly higher than the O₂ concentration, i.e. [O₂] = 2.4 mM^[26] vs. [DIPEA] > 140 mM, the diffusion-controlled eT by DIPEA is outcompeting any O₂ quenching of the triplet state in the beginning of the reaction and, thus, the drop in the initial catalytic efficiency under aerobic conditions results from the reaction of O₂ with the dFl semiquinone form, re-oxidising the dFl[•]. Hence, the used reaction conditions allow for efficient photocatalytic transformation of the substrate at least partially outcompeting potential undesired reactions with molecular oxygen.

The aerobic conditions can also be used for efficient dehalogenation on a preparative scale. For example, good dehalogenation product yields could be obtained after photo-reduction of **18** and **20** by **10a** (-H) or **10d** (o-Br) regardless on the molecular oxygen concentration (Table 3).

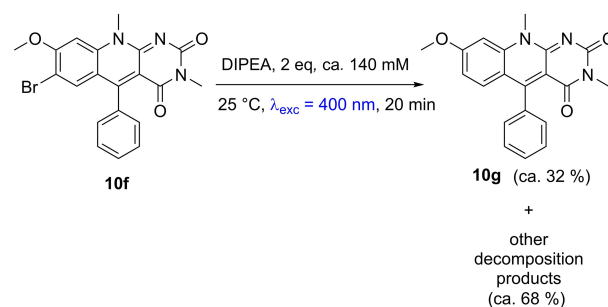
Influence of the bromine position on the photophysics of dFl 10. The energy for the first electronic transition, $E_{0,0}$, of all dFls have a higher energy gap by 0.2–0.35 eV between the ground and first excited singlet state compared to tetraacetylriboflavin (TARF, see Figure S17 in the Supporting Information). The variants with two MeO groups in the deazaisoalloxazine core, i.e., **10a** (-H), **10c** (p-Br), and **10d** (o-Br), have all a $E_{0,0}$ around 2.7 eV, thus, indicating that the bromination in the phenyl-side group does not have any influence on the transition energy.

However, among the dFls with two MeO groups, **10d** with the bromine in ortho position of the phenyl ring shows significantly altered photophysics in terms of a 50% higher fluorescence quantum yield (see Figure S17 in the Supporting Information), a 30% higher triplet yield (see Figure 2), and a five times longer excited singlet state lifetime compared to **10a** (-H) and **10c** (p-Br) (see Figure S17, Table S2, and further details in the Supporting Information). Quantum-mechanical calculations reveal that the significantly enhanced ISC in **10d** compared to **10a** and **10c** is explained by: i) a more favoured molecular orbital situation participating in the electronic transitions and ii) a beneficial steric situation in ortho position altering the torsion phenyl motion (for further details see Supporting Information and Figures S4–S6, S10–S12, and S16).

Substitution of one of the MeO groups by either H, Cl, or Br results in an increased transition energy $E_{0,0}$ by ca. 0.1 eV (see Figures S17 and S18 in the Supporting Information). Comparing all dFls the S₁ decay is shortest for **10f** (iso-Br) caused entirely

by triplet state formation (see Figure 2). While the S₁ of **10g** (iso-H, debromination product of **10f**, Scheme 3) decays with a lifetime of ca. 1 ns similarly to **10a** (-H) and **10c** (p-Br) – those without a bulky substituent in ortho position of the phenyl ring–, the S₁ lifetime of **10e** (iso-Cl) is by a factor of 2 longer. Considering also the triplet and fluorescence quantum yields for the iso substituted dFls, an IHAEC becomes evident. While the S₁ of **10a** (-H) mainly deactivates back to the ground state via internal conversion, the intersystem crossing becomes increasingly dominant from **10a** (-H) to **10f** (iso-Br) (see Figures 2 and S19 in the Supporting Information). In non-degassed ACN the triplet lifetimes for all dFls are very similar (see Figure S20 in the Supporting Information) and are mainly caused by bimolecular diffusion-controlled quenching by molecular oxygen as evident from the theoretically expected values (Table S3 in the Supporting Information). Table S2 in the Supporting Information summarises the photophysical parameters of all investigated dFls. In the absence of molecular oxygen (see Figure S21 in the Supporting Information), the dFls with two methoxy groups, i.e., **10a** (-H), **10c** (p-Br), and **10d** (o-Br), show a significantly enhanced triplet lifetime resembling the intrinsic triplet decay for these compounds. The lifetime of **10a** – the compound without heavy atom – is with 508 μs significantly longer than those observed for the two compounds with a bromine on the phenyl ring. Thus, for back ISC the bromine provides efficient SOC even if the bromine is located on the phenyl ring. Since the triplet yield of the dFls with only one methoxy group is much higher compared to the other dFls, a significantly higher transient triplet concentration may be reached in the absence of molecular oxygen under comparable excitation conditions. Accordingly, for **10g** (iso-H) and **10e** (iso-Cl) the formation of additional long-lived products via a triplet-triplet reaction is observed, which most likely corresponds to the radical ion pair as a result of electron transfer that recombines with a lifetime of ca. 500 μs in both cases. For **10f** (iso-Br) no further species are detected arising from the triplet decay because of the much more efficient SOC so that the intrinsic back ISC is completed with a lifetime of 55 μs outcompeting a potential reactive triplet-triplet encounter under these experimental conditions.

Ability to avoid the loss channel reaction via enhanced ISC. In the first step of the conPET reaction, spin-correlation of



Scheme 3. Debromination of **10f** (iso-Br) due to its photoinstability. Conditions: **10f** (0.003 mmol, ca. 6 mM), DIPEA (0.072 mmol, ca. 140 mM), ACN (0.5 mL), $T = 25\text{ }^{\circ}\text{C}$, argon atmosphere, $\lambda_{\text{exc}} = 400\text{ nm}$.

Table 3. Yields of the isolated dehalogenation products of **18** and **20** by **10a** (-H) or **10d** (o-Br) on a preparative scale.^[a]

Substrate	18	20
Catalyst	Yields [%] under argon/air	
10a (-H)	65/60	90/63
10d (o-Br)	80/58	81/68

[a] Reaction conditions: **18** or **20** (0.78 mmol, ca. 238 mM), **10a** or **10d** (0.062 mmol, ca. 19 mM), DIPEA (1.56 mmol, ca. 485 mM), ACN (3.0 mL), Cs₂CO₃ (0.78 mmol, ca. 238 mM), $T = 25\text{ }^{\circ}\text{C}$, argon/air atm., $\lambda_{\text{exc}} = 400\text{ nm}$, $t_{\text{rea}} = 24\text{ h}$.

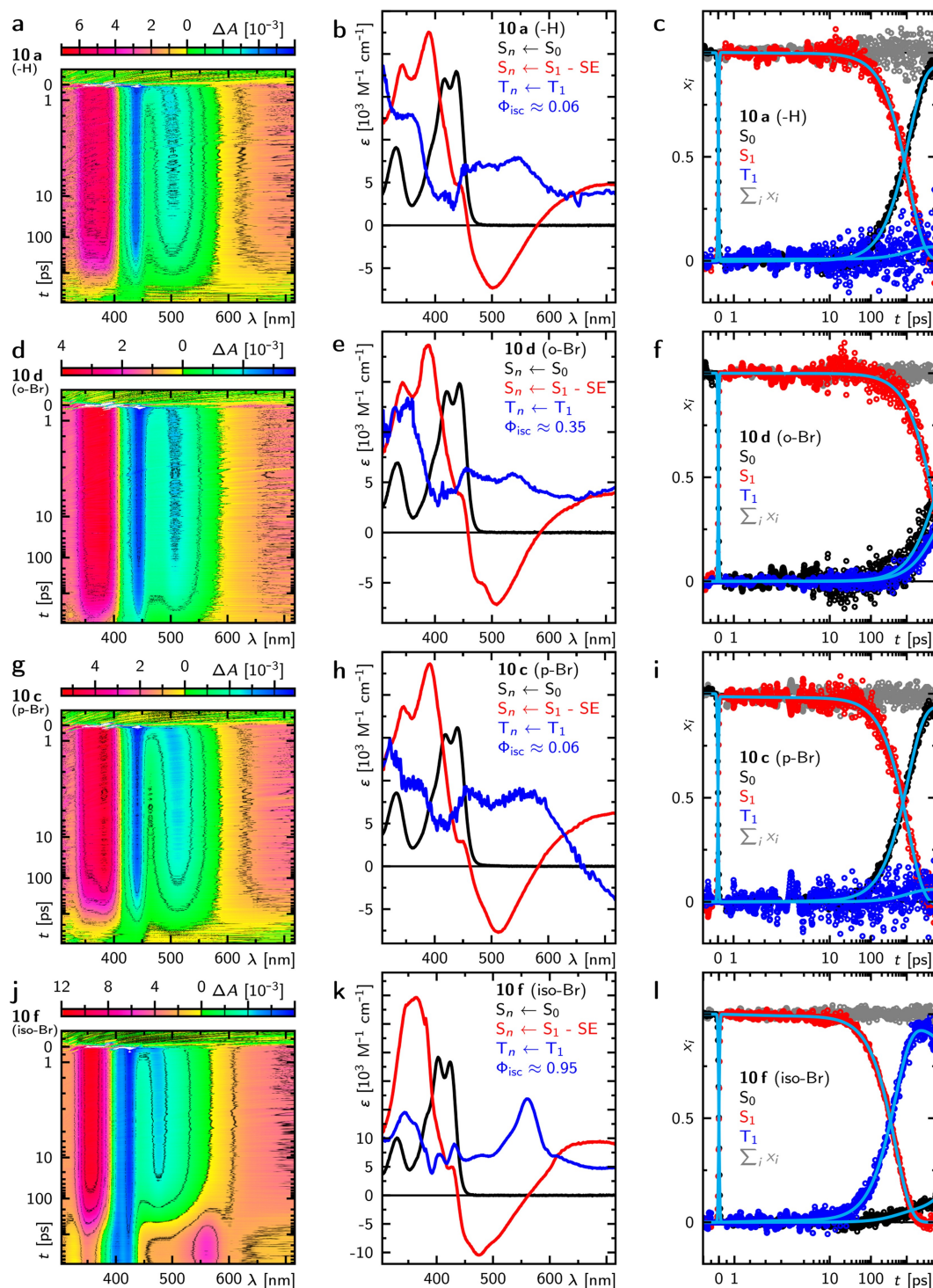


Figure 2. Excited singlet and triplet state dynamics of **10a** (-H, a–c), **10d** (o-Br, d–f), **10c** (p-Br, g–i), and **10f** (iso-Br, j–l) in ACN. a,d,g,j: False colour representation of the time-resolved absorption spectra excited into the $S_1 \leftarrow S_0$ transition at $\lambda_{\text{exc}} = 395$ nm. b,e,h,k: Species associated spectra (SAS) that contribute to the time-resolved absorption signals in panels a, d, g, and j with triplet quantum yields as indicated (for more details see Supporting Information). c,f,i,l: Corresponding concentration-time profiles of the SAS.

the initially formed radical pair plays a major role for the productive outcome. Thus, the concentration of the sacrificial electron donor DIPEA represents a crucial factor. As evident from Figure 3, at 500 mM DIPEA the dFIs **10a** (-H), **10c** (p-Br),

and **10d** (o-Br) undergo efficient and complete diffusion-controlled electron transfer forming the singlet-born radical pair that recombines faster than it is formed (see also Figures S23–S24 and further details in the Supporting Information, $S_n \leftarrow S_1$

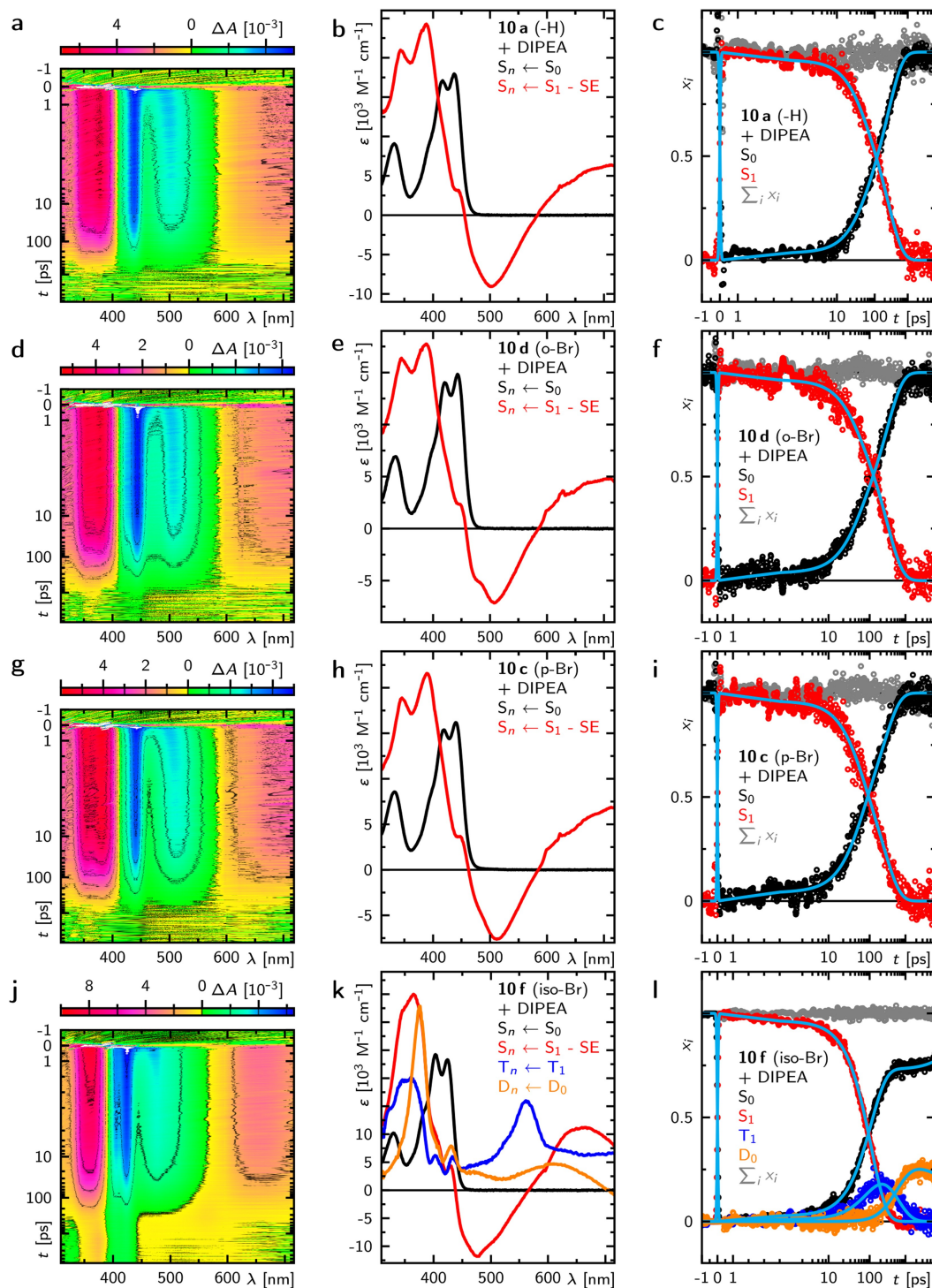


Figure 3. Transient absorption data of **10a** (-H, a–c), **10d** (o-Br, d–f), **10c** (p-Br, g–i), and **10f** (iso-Br, j–l) in ACN in the presence of 500 mM DIPEA. a,d,g,j: False colour representation of the time-resolved absorption spectra excited into the $S_1 \leftarrow S_0$ transition at $\lambda_{\text{exc}} = 395$ nm. b,e,h,k: Species associated spectra (SAS) that contribute to the time-resolved absorption signals in panels a, d, g, and j. c,f,i,l: Corresponding concentration-time profiles of the SAS.

plus stimulated emission (SE) giving a negative signal). Consequently, under this condition the systems follow the unproductive pathway via the excited singlet reaction and, thus, no dehalogenation is observed. The situation is different in case of **10f** (iso-Br). Here, the ISC is so enhanced that even at

500 mM DIPEA a significant quantity of triplet is formed (blue spectrum in Figure 3k, $T_n \leftarrow T_1$). Subsequently, the triplet reacts with DIPEA forming the triplet-born radical pair that is now detectable due to its spin-forbiddingness for recombination. To note, the counter DIPEA radical cation does not absorb in this

spectral range (Figure S24f) so that only the absorption spectrum of the **dFI**⁹ is observed (orange spectrum in Figure 3k, $D_n \leftarrow D_0 = {}^3[\text{dFI}_{\text{sq}}\text{S}_{\text{SAC}}^{\text{O}^+}]$). This demonstrates the relevance of the spin-correlation for the productive outcome in one single data set (Figure 3j).

Unfortunately, **10f** shows a significant photodecomposition at prolonged intense illumination. On an analytic scale, after 20 min of irradiation in the absence of halogenarene, **10f** photodecomposed completely. The main decomposition product could be assigned to 8-methoxydeazaflavin **10g** (*iso*-H) by MS and ¹H NMR (see Figures S25, S26, and S38 as well as further details in the Supporting Information) and yielded 32% in the preparative ansatz (Scheme 3). To note, when using 8 mol% of the photocatalyst, a higher yield for the dehalogenation of **14** after 24 h of illumination was achieved with **10g** compared to **10f** (see Table 1). However, considering that **10f** photodecomposes with 32% into **10g**, we performed the photodehalogenation with 2.6 mol% of **10g** (equal to 32% of the 8 mol% standard condition) which resulted in a similar course of the reaction and product yield as compared to the reaction with 8 mol% **10f** (see Figure S31). Thus, it is tempting to speculate that the other decomposition products (not identified) of **10f** do not contribute to the dehalogenation reaction. **10e** (*iso*-Cl) also showed a significant amount of photodecomposition (see Figures S27 and S28 in the Supporting Information). In contrast, the **dFIs** **10c** (*p*-Br) and **10d** (*o*-Br), i.e., with the halogen atom on the phenyl ring, show only a small amount of the dehalogenated compound **10a** (-H) after 20 min of irradiation (see Figures S29 and S30 in the Supporting Information). Thus, although **10f** provides the most beneficial photophysical characteristics compared to the other **dFIs**, as its bromine electron density participates in the electronic transitions to the excited states providing efficient triplet formation (see Figure S8 in the Supporting Information), the decomposition pathway via dissociation of the labile bromine group represents a drawback in the preparative usage.

As a compromise between photostability and triplet yield, **10d** and **10e** both perform very efficient in the debromination of bromoarenes. However, dechlorination is significantly less productive for **10e** (Table 1). Since **10e** consists of only one MeO group in the deazaisoalloxazine core, it is tempting to speculate that this structural difference will impact on other unproductive side reactions such as disproportionation, re-oxidation by molecular oxygen, eT from the excited state intermediate radical **dFI** to the substrate, and its lower photostability. The origin of the differential performance caused by the different structural motives is currently investigated in our labs and will be addressed elsewhere.

Avoiding the loss channel via the S₁ reaction by reduced concentration of the sacrificial electron donor. The diffusion-controlled bi-molecular rate constants for the unproductive S₁ reaction between DIPEA and the S₁ of **10a** (-H), **10d** (*o*-Br), **10g** (*iso*-H), and **10e** (*iso*-Cl) were determined via fluorescence quenching in the low concentration limit to $(1.13 \pm 0.02) \cdot 10^{10} \text{ M}^{-1} \cdot \text{s}^{-1}$, $(7.64 \pm 0.05) \cdot 10^9 \text{ M}^{-1} \cdot \text{s}^{-1}$, $(1.15 \pm 0.03) \cdot 10^{10} \text{ M}^{-1} \cdot \text{s}^{-1}$, and $(9.6 \pm 0.1) \cdot 10^9 \text{ M}^{-1} \cdot \text{s}^{-1}$, respectively (see Figure S22 and further information in the Supporting Informa-

tion). Comparison of these rates with the theoretical totally diffusion controlled bi-molecular rate constants estimated by the Smoluchowski theory (see Table S3 in the Supporting Information), may indicate a preference on reactive encounters in all cases as only 62%, 42%, 64%, and 53%, respectively, of collisions lead to a reaction. To note, bromination in the ortho position of the phenyl ring, as in **10d**, reduces the eT reaction efficiency on encounter with DIPEA by ca. 10–20% compared to the other **dFIs**. Since this unproductive reaction is entirely reversible, the amount of DIPEA will not be consumed by this reaction but the overall conversion velocity of the actual substrate will be significantly slowed down and will eventually stop at very high DIPEA concentrations. To demonstrate this, we determined the photodehalogenation efficiency of all relatively photostable **dFI** after 1 h illumination as a function of the DIPEA concentration for the exemplary conversion of **14** to **22** (Figure 4). The **dFIs** **10e** and **10g** with only one MeO group in the deazaisoalloxazine core show the lowest performance with a broad optimal range between 90 and 230 mM at a maximal conversion of around 15%. The **dFIs** with a second MeO group in the deazaisoalloxazine core perform consistently better reaching maxima of ca. 25% for **10a** and **10c** and of ca. 35% for **10d**. While the efficiency curve of **10c** shows a broad optimal range as obtained for **10g** and **10e**, the curve is significantly narrower and its maxima peak at around 60 mM (ca. 1 eq of **14**) for **10a** and **10d**. Although **10a** and **10c** underlie similar photophysical characteristics (see Supporting Information), the structural difference, i.e., the bromine in para position of the phenyl moiety, impacts on other unproductive side reactions as also discussed above. **10d** shows the best performance at optimal conditions in agreement with its altered photophysics and eT with DIPEA, as becomes obvious in a longer excited singlet state lifetime, a higher triplet yield, and a 20% less effective eT efficiency in the S₁ reaction with DIPEA.

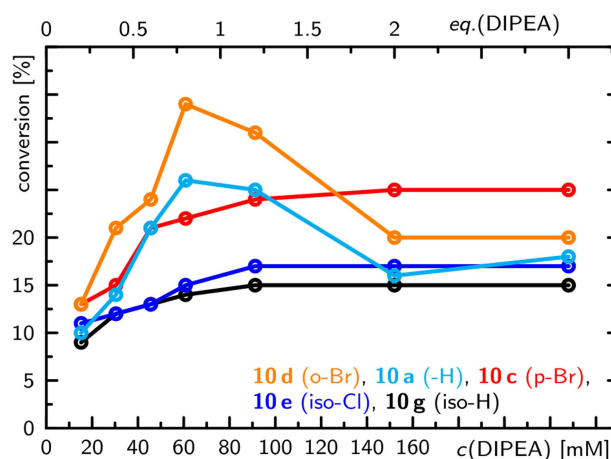


Figure 4. Product yield of anisole (**22**) after photocatalytic dehalogenation of bromoanisole (**14**) by selected **dFIs** **10** after 1 h of irradiation in dependence on the DIPEA concentration. Reaction conditions: **10** (0.003 mmol, ca. 6 mM), **14** (0.04 mmol, ca. 76 mM), DIPEA (0.008–0.114 mmol, ca. 15.2 to 228 mM), ACN (0.5 mL), Cs₂CO₃ (0.038 mmol, ca. 73 mM), T = 25 °C, under argon atmosphere, $\lambda_{\text{exc}} = 400 \text{ nm}$.

To point out, all dFIs clearly show a bell-shaped dependence, where the optimal DIPEA concentration lies below 240 mM, upon which the efficiency decreases due to contributions of the unproductive S_1 reaction via a singlet-born radical pair. Such a behaviour clearly indicates the involvement of the triplet state as a key intermediate^[27] in the underlying *conPET* reaction, thus, demonstrating the importance of the concentration conditions rather than considering only the equivalents of the sacrificial electron donor used in the system.

Conclusion

Here, we describe the successful synthesis of 5-aryldeazaflavins with Br or Cl substituents on different structural positions, i.e., on the phenyl side group or on the deazaalloxazine moiety, via three-component reactions and show their efficient usage as reductive photocatalysts enabling dehalogenation of bromo- and chloroarenes with electron-donating methoxy and alkyl groups even under aerobic conditions. The reductive power of the novel dFIs is comparable to that of sodium and lithium as demonstrated by the defluorination of 1,2-difluorobenzene and dechlorination of chlorobenzenes whose reduction is deactivated by methoxy and alkyl groups.

The synthesis was guided by mechanistic investigations aiming to increase ISC by the IHAIE within the dFIs, since the triplet state of the dFIs is the first crucial intermediate in the productive photocatalytic reaction based on the *conPET* mechanism, while the excited singlet state undergoes unproductive eT reactions with the sacrificial electron donor via a spin-correlated singlet-born radical pair that recombines faster

than it is formed (Figure 5).^[23] Introducing a bromine into the deazaalloxazine core has optimal impact on the triplet formation, i.e., almost 100%, but simultaneously also causes photo-instability and enhances other unproductive side reactions losing the advantage of the improved triplet yield. In contrast, positioning a bromine on the phenyl-side group did not affect the photostability by impacting on the triplet yield in dependence on the location within the phenyl ring. While a bromine in para position of the phenyl side group does not provide significant SOC to the system resulting in unaltered ISC, substitution on the ortho position resulted in a decent increase of the triplet yield, thus, providing – in a compromise between photostability and improved triplet yield formation – the best performance. Importantly, the performance of the photocatalytic process is further optimised by reducing the concentration of the sacrificial electron donor so that the unproductive S_1 reaction and the productive T_1 reactions are maximally avoided and enforced, respectively. This last point demonstrates the importance of the concentration conditions rather than equivalent relations of the sacrificial electron donor. Thus, in preparative applications the reductive conversions described here should be conducted under continuous addition of the sacrificial electron donor maintaining its actual concentration on a constant optimal level for maximal efficiency.

Another aspect of general importance for all *conPET* type reactions, as we have already stated in our previous work,^[23] is the specific timing of the two differently coloured intense photons necessary to be absorbed by the two key photocatalytic forms of the deazaflavins, where one is formed from the other having a distinct lifetime in the ns regime. Further experiments that provide insights for improvement on the

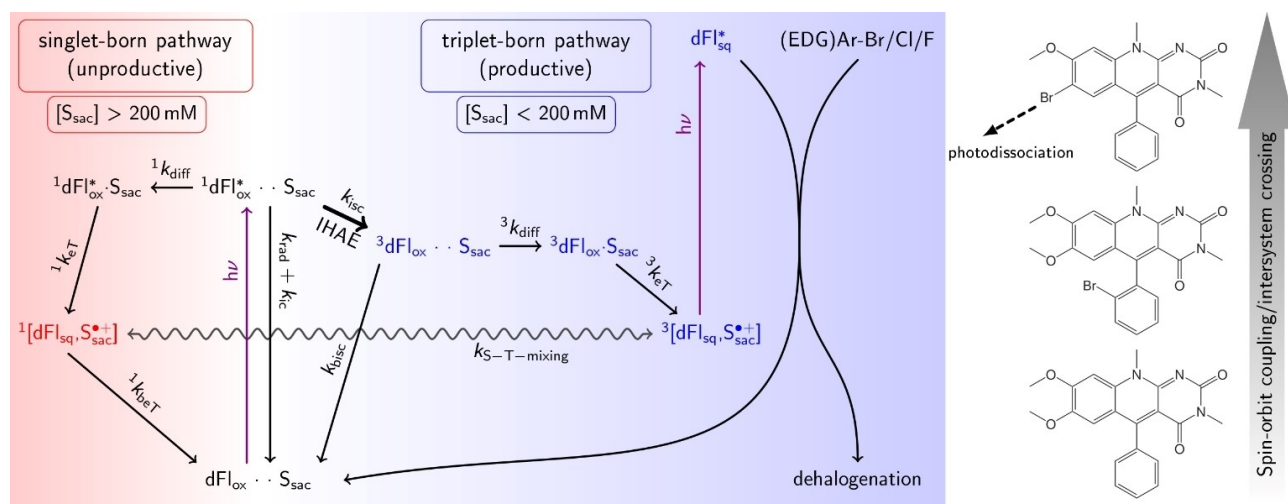


Figure 5. Photocatalytic reaction mechanism in a Jablonski type diagram (left, vertical axis represents a relative energy scale) and the structures of photocatalysts with increasing IHAIE (right). DIPEA as a sacrificial electron donor (S_{sac}) reacts either with the excited singlet or triplet state of the deazaflavin initiating either the unproductive (red) or productive (blue) pathway. In the unproductive pathway a singlet-born spin-correlated radical pair, $^1[\text{dFI}_{\text{sq}}\text{S}_{\text{sac}}^{\bullet+}]$, is formed after eT, which recombines faster than it is formed. In contrast, in the productive pathway eT to the triplet state results in a triplet-born radical pair, $^3[\text{dFI}_{\text{sq}}\text{S}_{\text{sac}}^{\bullet+}]$, allowing the accumulation of the considerably stable dFI_{sq} . A second photon can be absorbed by dFI_{sq} enabling a consecutive photo-induced electron transfer from dFI_{sq}^* to the substrate, (EDG)Ar–Br/Cl/F, regenerating dFI_{ox} in its ground state, closing the photocatalytic cycle, and initiating dehalogenation. The concentration of S_{sac} is decisive on the systems' reaction pathway, where the enhancement of the ISC by the IHAIE promotes the productive pathway via the triplet manifold. Bromine in the deazaalloxazine moiety provides maximal ISC, but photodissociates after prolonged illumination.

efficiency in terms of external experimental conditions are currently performed in our labs and will be published elsewhere.

This study demonstrates the importance of a detailed mechanistic understanding for the cost efficient and sustainable development of photocatalysts of the next generation. By our newly engineered deazaflavin photocatalysts, we expanded the photocatalytic toolbox for reductive conversions, where reduction powers comparable to that of sodium and lithium are required. Furthermore, the in-depth elucidation of the underlying mode of action of the *con*PET reaction will allow the projection onto other systems enabling their significant improvement.

Experimental Section

Extended information on materials and methods are described in the Supporting Information including detailed descriptions of the synthesis, NMR/Mass characterisation, time-resolved spectroscopic experimental setups and conditions, analysis, computational studies, extended references, and further supportive experimental work and collected data.

Acknowledgements

This project was supported by the Czech Science Foundation (Grant No. 19-09064S). Open Access funding enabled and organized by Projekt DEAL.

Conflict of Interest

The authors declare no conflict of interest.

Data Availability Statement

The data that support the findings of this study are available from the corresponding authors upon reasonable request.

Keywords: electron transfer · heavy atom effect · photocatalysis · reduction chemistry · spin-correlation

- [1] a) G. E. M. Crisenza, P. Melchiorre, *Nat. Commun.* **2020**, *11*, 803; b) T. Bach, *Angew. Chem. Int. Ed.* **2015**, *54*, 11294–11295; *Angew. Chem.* **2015**, *127*, 11448–11449; c) B. König, *Eur. J. Org. Chem.* **2017**, *2017*, 1979–1981; d) S. P. Pitre, L. E. Overman, *Chem. Rev.* **2022**, *122*, 1717–1751.
- [2] a) Y. Lee, M. S. Kwon, *Eur. J. Org. Chem.* **2020**, *2020*, 6028–6043; b) D. Petzold, M. Giedyk, A. Chatterjee, B. König, *Eur. J. Org. Chem.* **2020**, *2020*, 1193–1244; c) L. Marzo, S. K. Pagire, O. Reiser, B. König, *Angew. Chem. Int. Ed.* **2018**, *57*, 10034–10072; *Angew. Chem.* **2018**, *130*, 10188–10228; d) M. H. Shaw, J. Twilton, D. W. C. MacMillan, *J. Org. Chem.* **2016**, *81*, 6898–6926; e) R. C. McAtee, E. J. McClain, C. R. J. Stephenson, *Trends Chem.* **2019**, *1*, 111–125; f) J. J. Douglas, M. J. Sevrin, C. R. J. Stephenson, *Org. Process Res. Dev.* **2016**, *20*, 1134–1147.
- [3] a) N. A. Romero, D. A. Nicewicz, *Chem. Rev.* **2016**, *116*, 10075–10166; b) L. Buzzetti, G. E. M. Crisenza, P. Melchiorre, *Angew. Chem. Int. Ed.* **2019**, *58*, 3730–3747; *Angew. Chem.* **2019**, *131*, 3768–3786; c) L.

- Capaldo, D. Ravelli, *Eur. J. Org. Chem.* **2020**, *2020*, 2783–2806; d) D. Ravelli, S. Protti, M. Fagnoni, *Chem. Rev.* **2016**, *116*, 9850–9913.
- [4] a) M. Majek, A. Jacobi von Wangelin, *Acc. Chem. Res.* **2016**, *49*, 2316–2327; b) I. Ghosh, L. Marzo, A. Das, R. Shaikh, B. König, *Acc. Chem. Res.* **2016**, *49*, 1566–1577; c) M. Neumeier, D. Sampedro, M. Májek, V. A. d. I. P. O'Shea, A. J. v. Wangelin, R. Pérez-Ruiz, *Chem. Eur. J.* **2018**, *24*, 105–108.
- [5] a) D. Kalyani, K. B. McMurtrey, S. R. Neufeldt, M. S. Sanford, *J. Am. Chem. Soc.* **2011**, *133*, 18566–18569; b) D. P. Hari, P. Schroll, B. König, *J. Am. Chem. Soc.* **2012**, *134*, 2958–2961; c) J. D. Nguyen, E. M. D'Amato, J. M. R. Narayanam, C. R. J. Stephenson, *Nat. Chem.* **2012**, *4*, 854–859.
- [6] a) Y. Du, R. M. Pearson, C. H. Lim, S. M. Sartor, M. D. Ryan, H. Yang, N. H. Damrauer, G. M. Miyake, *Chem. Eur. J.* **2017**, *23*, 10962–10968; b) M. Marin, M. A. Miranda, M. L. Marin, *Catal. Sci. Technol.* **2017**, *7*, 4852–4858.
- [7] a) S. O. Poelma, G. L. Burnett, E. H. Discekici, K. M. Mattson, N. J. Treat, Y. Luo, Z. M. Hudson, S. L. Shankel, P. G. Clark, J. W. Kramer, C. J. Hawker, J. Read de Alaniz, *J. Org. Chem.* **2016**, *81*, 7155–7160; b) E. H. Discekici, N. J. Treat, S. O. Poelma, K. M. Mattson, Z. M. Hudson, Y. Luo, C. J. Hawker, J. R. de Alaniz, *Chem. Commun.* **2015**, *51*, 11705–11708; c) N. Noto, Y. Tanaka, T. Koike, M. Akita, *ACS Catal.* **2018**, *8*, 9408–9419; d) B. G. McCarthy, R. M. Pearson, C.-H. Lim, S. M. Sartor, N. H. Damrauer, G. M. Miyake, *J. Am. Chem. Soc.* **2018**, *140*, 5088–5101.
- [8] J.-H. Shon, D. Kim, M. D. Rathnayake, S. Sittel, J. D. Weaver, T. S. Teets, *Chem. Sci.* **2021**, *11*, 4069–4078.
- [9] a) R. Cibulka, *Nature* **2020**, *580*, 31–32; b) N. E. S. Tay, D. Lehnher, T. Rovis, *Chem. Rev.* **2022**, *122*, 2487–2649; c) J. Liu, L. Lu, D. Wood, S. Lin, *ACS Cent. Sci.* **2020**, *6*, 1317–1340.
- [10] I. Ghosh, T. Ghosh, J. I. Bardagi, B. König, *Science* **2014**, *346*, 725–728.
- [11] a) I. Ghosh, B. König, *Angew. Chem. Int. Ed.* **2016**, *55*, 7676–7679; *Angew. Chem.* **2016**, *128*, 7806–7810; b) L. Marzo, I. Ghosh, F. Esteban, B. König, *ACS Catal.* **2016**, *6*, 6780–6784; c) J. I. Bardagi, I. Ghosh, M. Schmalzbaue, T. Ghosh, B. König, *Eur. J. Org. Chem.* **2018**, *2018*, 34–40.
- [12] I. A. MacKenzie, L. Wang, N. P. R. Onuska, O. F. Williams, K. Begam, A. M. Moran, B. D. Dunietz, D. A. Nicewicz, *Nature* **2020**, *580*, 76–80.
- [13] a) J. Xu, J. Cao, X. Wu, H. Wang, X. Yang, X. Tang, R. W. Toh, R. Zhou, E. K. L. Yeow, J. Wu, *J. Am. Chem. Soc.* **2021**, *143*, 13266–13273; b) A. F. Chmiel, O. P. Williams, C. P. Chernowsky, C. S. Yeung, Z. K. Wickens, *J. Am. Chem. Soc.* **2021**, *143*, 10882–10889.
- [14] N. G. W. Cowper, C. P. Chernowsky, O. P. Williams, Z. K. Wickens, *J. Am. Chem. Soc.* **2020**, *142*, 2093–2099.
- [15] H. Kim, H. Kim, T. H. Lambert, S. Lin, *J. Am. Chem. Soc.* **2020**, *142*, 2087–2092.
- [16] J. P. Cole, D.-F. Chen, M. Kudisch, R. M. Pearson, C.-H. Lim, G. M. Miyake, *J. Am. Chem. Soc.* **2020**, *142*, 13573–13581.
- [17] F. Glaser, C. B. Larsen, C. Kerzig, O. S. Wenger, *Photochem. Photobiol. Sci.* **2020**, *19*, 1035–1041.
- [18] a) J. B. Metternig, R. J. Mudd, G. R., in *Photocatalysis in Organic Synthesis*, 2019 ed. (Ed.: B. König), Georg Thieme Verlag, Stuttgart, **2019**, pp. 391–404; b) B. König, S. Kümmel, E. Svobodová, R. Cibulka, in *Phys. Sci. Rev., Vol. 3*, **2018**; c) I. K. Sideri, E. Voutyritsa, C. G. Kokotich, *Org. Biomol. Chem.* **2018**, *16*, 4596–4614; d) V. Srivastava, P. K. Singh, A. Srivastava, P. P. Singh, *RSC Adv.* **2021**, *11*, 14251–14259; e) A. Rehpen, A. Walter, G. Storch, *Synthesis* **2021**, *53*, 2583–2593.
- [19] a) A. Pokluda, Z. Anwar, V. Boguschová, I. Anusiewicz, P. Skurski, M. Sikorski, R. Cibulka, *Adv. Synth. Catal.* **2021**, *363*, 4371–4379; b) T. Hartman, M. Reiserová, J. Chudoba, E. Svobodová, N. Archipowa, R. J. Kutta, R. Cibulka, *ChemPlusChem* **2021**, *86*, 373–386; c) D.-M. Răsădean, T. Machida, K. Sada, C. R. Pudney, G. D. Pantoş, *Tetrahedron* **2021**, *131925*; d) A. H. Tolba, M. Krupička, J. Chudoba, R. Cibulka, *Org. Lett.* **2021**, *23*, 6825–6830; e) H. Guo, H. Xia, X. Ma, K. Chen, C. Dang, J. Zhao, B. Dick, *ACS Omega* **2020**, *5*, 10586–10595; f) A. H. Tolba, F. Vávra, J. Chudoba, R. Cibulka, *Eur. J. Org. Chem.* **2020**, *2020*, 1579–1585; g) P. Thapa, S. Hazaar, B. Chouhan, T. T. Vuong, F. W. Foss, *J. Org. Chem.* **2020**, *85*, 9096–9105; h) N. P. Ramirez, T. Lana-Villarreal, J. C. Gonzalez-Gomez, *Eur. J. Org. Chem.* **2020**, *2020*, 1539–1550; i) L. M. Bouchet, A. A. Heredia, J. E. Argüello, L. C. Schmidt, *Org. Lett.* **2020**, *22*, 610–614; j) J. Zelenka, E. Svobodová, J. Tarábek, I. Hoskovcová, V. Boguschová, S. Bailly, M. Sikorski, J. Roithová, R. Cibulka, *Org. Lett.* **2019**, *21*, 114–119; k) N. P. Ramirez, B. König, J. C. Gonzalez-Gomez, *Org. Lett.* **2019**, *21*, 1368–1373; l) T. Tagami, Y. Arakawa, K. Minagawa, Y. Imada, *Org. Lett.* **2019**, *21*, 6978–6982; m) M. März, M. Kohout, T. Nevesely, J. Chudoba, D. Prukala, S. Niziński, M. Sikorski, G. Burdziński, R. Cibulka, *Org. Biomol. Chem.* **2018**, *16*, 6809–6817; n) T. Nevesely, E. Svobodová, J. Chudoba,

- M. Sikorski, R. Cibulka, *Adv. Synth. Catal.* **2016**, *358*, 1654–1663; o) J. B. Metternich, R. Gilmour, *J. Am. Chem. Soc.* **2016**, *138*, 1040–1045.
- [20] a) R. Martínez-Haya, M. A. Miranda, M. L. Marin, *Eur. J. Org. Chem.* **2017**, 2164–2169; b) R. Foja, A. Walter, C. Jandl, E. Thyraug, J. Hauer, G. Storch, *J. Am. Chem. Soc.* **2022**, *144*, 4721–4726.
- [21] It should be noted that some photoenzymatic systems involving flavoenzymes could be used in photoreductions, see: a) B. A. Sandoval, P. D. Clayman, D. G. Oblinsky, S. Oh, Y. Nakano, M. Bird, G. D. Scholes, T. K. Hyster, *J. Am. Chem. Soc.* **2021**, *143*, 1735–1739; b) K. F. Biegasiwicz, S. J. Cooper, X. Gao, D. G. Oblinsky, J. H. Kim, S. E. Garfinkle, L. A. Joyce, B. A. Sandoval, G. D. Scholes, T. K. Hyster, *Science* **2019**, *364*, 1166–1169; c) B. T. Nicholls, D. G. Oblinsky, S. I. Kurtoic, D. Grosheva, Y. Ye, G. D. Scholes, T. K. Hyster, *Angew. Chem. Int. Ed.* **2022**, *61*, e202113842; *Angew. Chem.* **2022**, *134*, e202113842.
- [22] a) C. Greening, F. H. Ahmed, A. E. Mohamed, B. M. Lee, G. Pandey, A. C. Warden, C. Scott, J. G. Oakeshott, M. C. Taylor, C. J. Jackson, *Microbiol. Mol. Biol. Rev.* **2016**, *80*, 451–493; b) C. Walsh, *Acc. Chem. Res.* **1986**, *19*, 216–221; c) M. Goldberg, I. Pecht, H. E. A. Kramer, R. Traber, P. Hemmerich, *Biochim. Biophys. Acta Gen. Subj.* **1981**, *673*, 570–593; d) P. Hemmerich, V. Massey, H. Fenner, *FEBS Lett.* **1977**, *84*, 5–21.
- [23] A. Graml, T. Neveselý, R. J. Kutta, R. Cibulka, B. König, *Nat. Commun.* **2020**, *11*, 3174.
- [24] K. K. Kundu, A. K. Rakshit, M. N. Das, *Electrochim. Acta* **1972**, *17*, 1921–1937.
- [25] a) D. E. O'Brien, L. T. Weinslock, C. C. Cheng, *J. Heterocycl. Chem.* **1970**, *7*, 99–105; b) F. Yoneda, Y. Sakuma, S. Mizumoto, R. Ito, *J. Chem. Soc. Perkin Trans. 1* **1976**, 1805–1808; c) F. Yoneda, T. Asano, K. Tsukuda, A. Koshiro, *Heterocycles* **1979**, *12*, 691–694; d) M. S. Hossain, C. Q. Le, E. Joseph, T. Q. Nguyen, K. Johnson-Winters, F. W. Foss, *Org. Biomol. Chem.* **2015**, *13*, 5082–5085.
- [26] C. Franco, J. I. Olmsted, *Talanta* **1990**, *37*, 905–909.
- [27] U. Megerle, M. Wenninger, R.-J. Kutta, R. Lechner, B. König, B. Dick, E. Riedle, *Phys. Chem. Chem. Phys.* **2011**, *13*, 8869–8880.

Manuscript received: March 10, 2022

Accepted manuscript online: May 10, 2022

Version of record online: June 24, 2022